Axial Alignment for Anterior Segment Swept Source Optical Coherence Tomography via Robust Low-Rank Tensor Recovery

Yanwu Xu[1(✉)], Lixin Duan[2], Huazhu Fu[1], Xiaoqin Zhang[3], Damon Wing Kee Wong[1], Baskaran Mani[4], Tin Aung[4], and Jiang Liu[1,5]

[1] Institute for Infocomm Research, Agency for Science, Technology and Research, Singapore, Singapore
yaxu@i2r.a-star.edu.sg
[2] Amazon, Seattle, USA
[3] Wenzhou University, Wenzhou, China
[4] Singapore Eye Research Institute, Singapore, Singapore
[5] Cixi Institute of Biomedical Engineering, Ningbo Institute of Materials Technology and Engineering, Chinese Academy of Sciences, Ningbo, China

Abstract. We present a one-step approach based on low-rank tensor recovery for axial alignment in 360-degree anterior chamber optical coherence tomography. Achieving translational alignment and rotation correction of cross-sections simultaneously, this technique obtains a better anterior segment topographical representation and improves quantitative measurement accuracy and reproducibility of disease related parameters. Through its use of global information, the proposed method is more robust compared to using only individual or paired slices, and less sensitive to noise and motion artifacts. In angle closure analysis on 30 patient eyes, the preliminary results indicate that the proposed axial alignment method can not only facilitate manual qualitative analysis with more distinct landmark representation and much less human labor, but also can improve the accuracy of automatic quantitative assessment by 2.9 %, which demonstrates that the proposed approach is promising for a wide range of clinical applications.

1 Introduction

The optical system resides in the anterior segment of the human eye, which consists of the cornea, iris and crystalline lens, as shown in Fig. 1A and C. Pathological changes in this area can drastically degrade vision and even result in blindness [1–3]. Quantitative assessments of the anterior segment are thus essential to a wide range of clinical applications [2–5].

Nowadays swept source optical coherence tomography (SS-OCT) is the most advanced technology for eye imaging, which has significantly improved imaging

This work is funded by A*STAR BEP Grant (152 148 0034) and NSFC Grant (61511130084).

S. Ourselin et al. (Eds.): MICCAI 2016, Part III, LNCS 9902, pp. 441–449, 2016.
DOI: 10.1007/978-3-319-46726-9_51

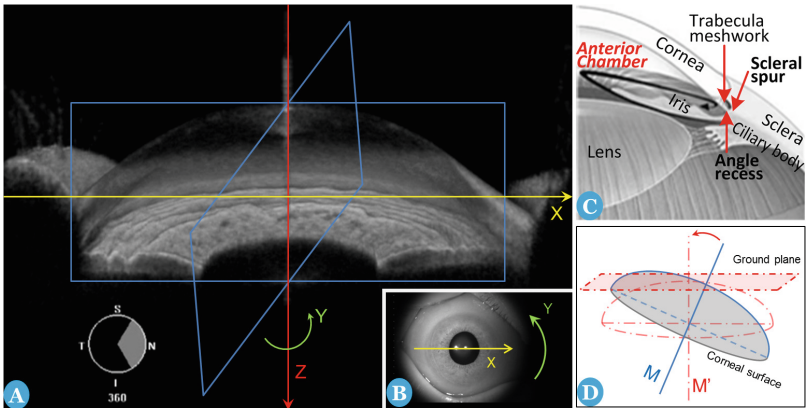

Fig. 1. A: swept source optical coherence tomography of anterior segment, where each *A-scan* is captured along the Z axis, each *B-scan* is captured along the X axis, and a 360-degree circular scan is performed along the Y axis. **B:** top view of the 360-degree anterior segment imaging process. **C:** anatomical structure of anterior segment around the angle. **D:** illustration of axial alignment of corneal surface reconstructed from aligned B-scans.

speed and detection sensitivity in comparison to traditional OCT technologies. Most recently, anterior segment SS-OCT (AS-SS-OCT) [1,6,7] has been developed for 3D imaging of the anterior segment of the human eye. Nevertheless, it is still hard to use SS-OCT to capture well-aligned B-scans along the X axis, due to involuntary eye motions and the relatively low density of raster scans.

As a fundamental problem for all SS-OCT based imaging technologies, *translational misalignment* reduction has been studied for SS-OCT retinal scans [8,9]. However, in the context of the anterior segment, we additionally need to correct the tilt of B-scans, due to the *rotational misalignment* caused by the positioning of an eye [10] and the fixation lag of the instrument [1] (which ignores eye movement during the imaging process [8,9]). As shown in Fig. 1D, the task is to tilt the axis M of the corneal surface to the ideal axis M' which is perpendicular to the ground plane. This is crucial to conduct accurate and reproducible quantitative measurements [1] of the anterior segment for various parameters that depend only on the actual geometry of the anterior chamber structure, e.g., cornea thickness map [1], central anterior chamber depth [2,3] and iris-trabecular contact (ITC) index [5].

To our knowledge, no such work has been done, although its importance has been highlighted in AS-SS-OCT instrument design works [1,6]. We formally refer to this problem as the *axial alignment* problem, which will be studied in this work. Currently, axial alignment and clinical parameter measurement rely on manual marking of landmarks (e.g., scleral spur [4,5]). And no fully automated approach has ever been reported. In this work, we propose a ***one-step*** method to simultaneously solve the alignment and rotation issues by using robust low-rank

tensor recovery, based on the symmetry characteristic of the anterior segment structure. Our proposed method effectively utilizes the global information from the entire volume to reduce the sensitivity to noise and blur, and generates more reliable and smooth results. Moreover, our method is able to solve other general alignment problems when the input data is represented by a tensor. To verify the effectiveness of the proposed axial alignment algorithm, we perform extensive experiments on anterior chamber angle (ACA) analysis to qualitatively and quantitatively examine the improvements from performing axial alignment.

2 Proposed Method

2.1 Problem Formulation

An AS-SS-OCT volume, consisting of n_3 cross-sectional slices, can be viewed as a 3D tensor (see the *left* of Fig. 2), denoted as $\mathcal{D} \in \mathbb{R}^{n_1 \times n_2 \times n_3}$, where n_i is a positive integer. An ideal 360-degree AS-SS-OCT scan does not contain any noise or artifacts and its cross-sectional slices are all well aligned with each other. And thus, the tensor representation of an AS-SS-OCT volume should exhibit a *low-rank* structure, which is denoted as $\mathcal{A}$. However, artifacts from the AS-SS-OCT machine and small disturbances of the eyes (e.g., the involuntary axial movement) during the scan process may break the low-rank structure. In this work, we propose an axial alignment method by recovering the ideal low-rank structure $\mathcal{A}$ from a real OCT volume tensor $\mathcal{D}$, by taking into account the imaging difference $\mathcal{E}$ as well as by introducing a set of transformations $\mathrm{T} = \{\boldsymbol{\tau}_1, \ldots, \boldsymbol{\tau}_{n_3}\}$ to correct the misalignment and rotation. With the above, mathematically we have:

$$\mathcal{D} \circ \mathrm{T} = \mathcal{A} + \mathcal{E}, \tag{1}$$

where $\mathcal{D} \circ \mathrm{T}$ means applying every transformation $\boldsymbol{\tau}_k$ to the corresponding OCT image $\mathcal{A}[:, :, k], k = 1, \ldots, n_3$. Additionally in this work, we assume that only a small fraction of the image pixels are corrupted by imaging artifacts, and hence $\mathcal{E}$ becomes a sparse error term. Therefore, with $\mathcal{A}$ being low-rank and $\mathcal{E}$ being sparse, we formally present the axial alignment problem as follows:

$$\min_{\mathcal{A}, \mathcal{E}, \mathrm{T}} \quad \mathrm{rank}(\mathcal{A}) + \lambda \|\mathcal{E}\|_0, \quad \text{s.t.} \quad \mathcal{D} \circ \mathrm{T} = \mathcal{A} + \mathcal{E}. \tag{2}$$

2.2 Solution

Note that it is not a trivial task to directly solve (2). Instead, we propose to decompose the rank of $\mathcal{A}$ by using the tensor rank definition [13] based on the Tucker decomposition [14]. Specifically, under the Tucker decomposition, $\mathcal{A}$ can be viewed as a rank-(r_1, r_2, r_3) tensor, where r_i is the rank of the unfolding matrix $\mathcal{A}_{(i)}$. And then $\mathrm{rank}(\mathcal{A})$ becomes a linear combination of $\mathrm{rank}(\mathcal{A}_{(i)})$'s, i.e., $\mathrm{rank}(\mathcal{A}) = \sum_{i=1}^{3} \omega_i \cdot \mathrm{rank}(\mathcal{A}_{(i)})$, where $\omega_i \in [0, 1]$ is the predefined weight

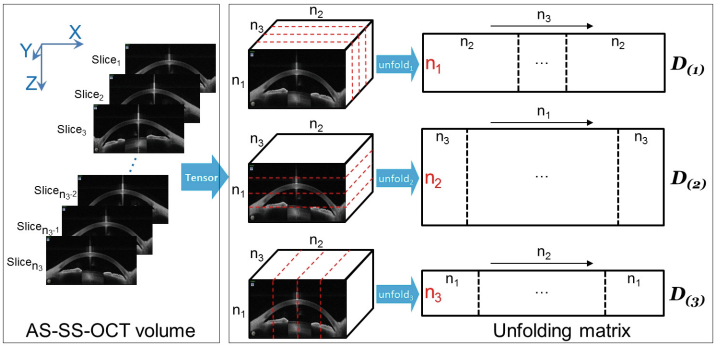

Fig. 2. *Left:* An AS-SS-OCT volume comprised of n_3 B-scans. *Right:* Tensor unfolding along each order

for the corresponding unfolding matrix $\mathcal{A}_{(i)}$, and $\sum_{i=1}^{3} \omega_i = 1$ is assumed to make the definition consistent with the form of the matrix. This decomposition step is essentially equivalent to first naturally unfolding the original tensor $\mathcal{A}$ to the unfolding matrices $\mathcal{A}_{(i)}$'s and then directly working on the combination of the ranks of $\mathcal{A}_{(i)}$'s. It is worth mentioning that minimizing the ranks of $\mathcal{A}_{(i)}$'s is intuitively meaningful in our studied problem. Specifically, enforcing the low rank of $\mathcal{A}_{(2)}$ and $\mathcal{A}_{(3)}$ will achieve good image alignment among the corresponding B-scans along the X and Z axes respectively, while keeping the low rank of $\mathcal{A}_{(1)}$ will correct the rotation of B-scans along the Z axis[1] [15]. So together, we can achieve both good image alignment and rotational correction in our axial alignment task for an input AS-SS-OCT volume.

Since it is still not easy to directly minimize $\sum_{i=1}^{3} \omega_i \cdot \text{rank}(\mathcal{A}_{(i)})$ (due to the nonconvexity and discontinuity of the rank operation), we propose to replace each rank operation by using the corresponding nuclear norm which is a convex approximation. As a result, we approximate $\text{rank}(\mathcal{A})$ by using:

$$\text{rank}(\mathcal{A}) = \sum_{i=1}^{3} \omega_i \cdot \text{rank}(\mathcal{A}_{(i)}) \approx \sum_{i=1}^{3} \omega_i \|\mathcal{A}_{(i)}\|_*. \tag{3}$$

Moreover, following [16], we replace the ℓ_0-norm in (2) with its convex surrogate ℓ_1-norm. In addition, since the constraint $\mathcal{D} \circ \mathrm{T} = \mathcal{A} + \mathcal{E}$ in (2) is non-linear, similar to [16], we approximate the constraint by linearizing it based on the first-order Taylor expansion (assuming the change in $\boldsymbol{\tau}_k$ is small). And together with (3), we approximate our original problem by using the following one:

$$\min_{\mathcal{A},\mathcal{E},\mathrm{T}} \sum_{i=1}^{3} \omega_i \|\mathcal{A}_{(i)}\|_* + \lambda \|\mathcal{E}\|_1, \text{ s.t. } \mathcal{D} \circ \mathrm{T} + \Delta\hat{\mathrm{T}} = \mathcal{A} + \mathcal{E}, \tag{4}$$

[1] As illustrated in Fig. 2, $\mathcal{A}_{(1)}$, $\mathcal{A}_{(2)}$ and $\mathcal{A}_{(3)}$ are obtained by unfolding $\mathcal{A}$ along the Z, X and Y axes, respectively.

where $\Delta\hat{\mathrm{T}} = \mathrm{fold}_3\Big(\big(\sum_{k=1}^{n_3} J_k \Delta\mathrm{T}\boldsymbol{\epsilon}_k\boldsymbol{\epsilon}_k^\top\big)^\top\Big)$, $\mathrm{fold}_3(\cdot)$ is the inverse operation of the mode-3 unfolding[2], J_k represents the Jacobian of $\mathcal{A}[:,:,k]$ *w.r.t.* the k-th transformation $\boldsymbol{\tau}_k$, and $\boldsymbol{\epsilon}_k$ denotes the standard basis.

To solve (4), we first introduce a matrix B_i to replace $\mathcal{A}_{(i)}$ for each i, which decouples the interdependencies among the $\mathcal{A}_{(i)}$'s and relaxes (4), and then we arrive at the following optimization problem:

$$\min_{\mathcal{A},\mathcal{E},\mathrm{T},B_i} \sum_{i=1}^{3} \omega_i \|B_i\|_* + \lambda\|\mathcal{E}\|_1, \text{ s.t. } B_i = \mathcal{A}_{(i)}, \mathcal{D}\circ\mathrm{T} + \Delta\hat{\mathrm{T}} = \mathcal{A}+\mathcal{E}. \quad (5)$$

The optimization problem in (5) can be solved by employing the augmented Lagrange multiplier (ALM) method [17]. After solving (5) to obtain the optimal T^*, we can effectively correct both the alignment and rotation of all the OCT images from a test OCT imaging volume $\mathcal{D}$, by performing $\mathcal{D}\circ\mathrm{T}^*$, which is also the final result of axial alignment for $\mathcal{D}$.

2.3 Discussion

The proposed method is a relatively generalized approach which can be extended to different use cases. For instance, single images can be rectified by setting $\omega_3 = 0$ or get aligned without the need of rotation correction by setting $\omega_1 = 0$. Also, since the tensor representation can be extended to a higher order, we may be able to align multiple volumes from different or the same eyes along the axial direction to facilitate comparison, and our method may have potential to become a platform for pathology discovery in a series of images from different time instances. Moreover, the obtained error term $\mathcal{E}^*$, after solving (2), can be used to (1) capture pixel-wise differences for image denoising, deblurring and corruption recovery; and (2) detect outliers caused by artifacts or lesions. We will consider the above mentioned use cases as our future work.

3 Experiments

Since anterior chamber angle (ACA) analysis is the major application of anterior segment imaging (which has attracted much attention from clinicians [2,3,5] and computer-aided-diagnosis researchers [11,12]), we employ it for performance measurement on axial alignment. Specifically, based on ACA analysis, we investigate different manual/semi-automatic and fully automatic methods, by performing both visual comparison and qualitative evaluation.

3.1 Dataset and Experimental Setup

A total of 30 AS-SS-OCT volumes of 30 patients' eyes are used for the experiment. Each volume contains 128 slices, and each slice captures two angles at a

[2] To give an example, the inverse operation of the mode-i unfolding on an unfolding matrix $\mathcal{A}_{(i)}$ restores the original tensor $\mathcal{A}$, i.e., $\mathcal{A} = \mathrm{fold}_i(\mathcal{A}_{(i)})$.

resolution of 1680×900. Among the 30 AS-SS-OCT volumes, 16 of them have primary angle closure (PAC) and the other 14 have open angle controls (OAC) [5,11,12]. For our method, we empirically set $\omega_1 = 0.5, \omega_2 = 0.25, \omega_3 = 0.25$ and $\lambda = 0.8$. On average, it takes about 20 mins to process each volume on a 3.2 GHz CPU with 24 GB RAM using MATLAB code. Optimizations for speed are certainly possible [17].

3.2 Qualitative Evaluation

The qualitative evaluation is based on each single volume. The corresponding 128 slices of a volume are averaged before and after axial alignment in order to visually compare whether it can help identify PAC and OAC. In current clinical practice, this task totally relies on manual assessment, i.e., for each 360-degree scan, the ophthalmologists manually mark the landmarks (seen in Fig. 1C) such as scleral spur (SS) and angle recess (AR) on four or more slices, to calculate parameters such as ITC index [5] (which needs axial adjustment), angle opening distance (AOD) [3], etc., or directly classify each angle as open or closed. As reported in [5], at least 16 labeled slices (32 angles) are required to guarantee a relatively reliable angle closure grading, which is very time consuming and subjective, and may be inaccurate due to a low sampling ratio.

As illustrated in Fig. 3, it is clear that in general the averaged slices after axial alignment are visually much better than the ones before axial alignment, which provides a clearer *summarization* of each AS-SS-OCT volume to facilitate qualitative assessment of angle closure, with much less human labor involved, compared to conventional practice (1 vs 16+). Note that among the six averaged aligned slices, Fig. 3C_2 still has a bit of blurring at the iris regions. This is due to the considerable scale change caused by bad eye positioning (i.e., imaging does not focus on or aim at the geometrical corneal center), which unfortunately cannot be recovered without introducing distortion.

In addition, as reported in [4], previously the SS points could not even be manually located in 30 % or more of angles, which greatly hampers quantitative analysis of a large number of ACA parameters related to SS [3,4]. However, as demonstrated in Fig. 3, the SS points are more distinct in well-aligned averaged cross-sectional slices. This not only can facilitate manual or semi-automatic quantitative analysis, but may also be used to develop a new fully automatic quantitative measurement tool for angle closure assessment, which will be investigated in our future work.

3.3 Quantitative Evaluation

The quantitative experiments are based on classifying each individual angle to open or closed, and the ground truth of the 7680 angles is labeled by a group of ophthalmologists from a hospital. The ITC in each ACA is located using the algorithm proposed in [12], and then a linear SVM classifier is used to classify each angle as open or closed, using HOG or HEP features as proposed in [11, 12], respectively. We compare the classification accuracy before and after axial

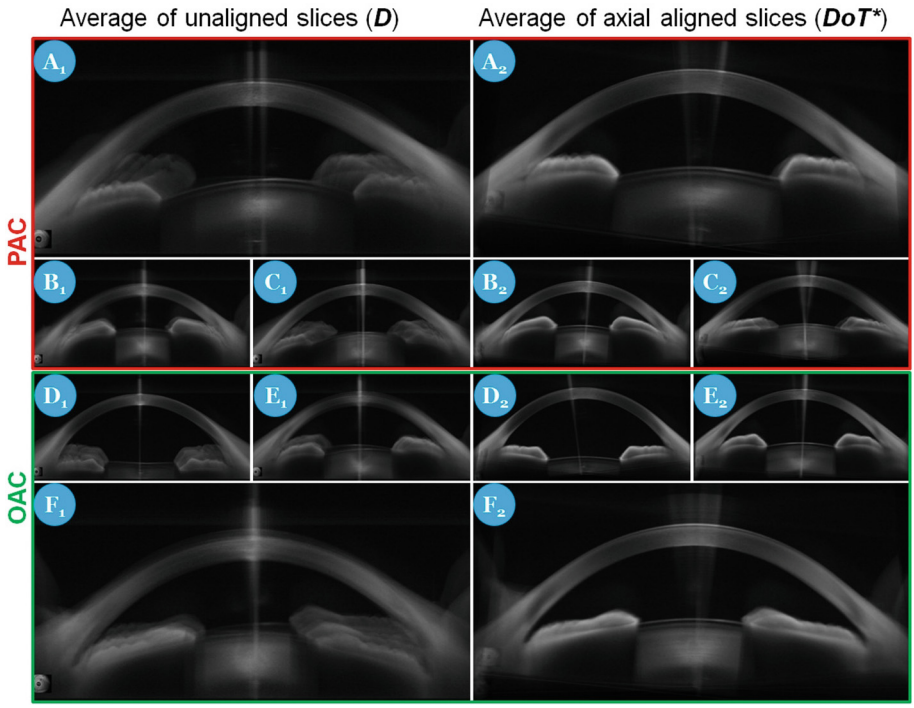

Fig. 3. Illustration of averaged cross-sectional slices before (*left column*) and after (*right column*) axial alignment.

alignment to investigate how the proposed axial alignment facilitates automatic ACA classification.

We performed ten repeated 2-fold cross-validation experiments, *i.e.*, for each testing round, half of all the volumes with PAC and OAC are randomly selected to train a classifier, and the other half are used for testing; then the training and testing data are swapped to perform the test again. We assess the performance using balanced accuracy ($\bar{P}$) with a fixed 85 % specificity (P_{-}) and area under ROC curve (AUC) which evaluates the overall performance. The optimal parameters of each method are chosen following [11,12]. For more details, readers may refer to [11,12].

Table 1. Performance comparisons for ACA classification before and after axial alignment (denoted as $AL+$ in the table) (P-value < 0.01)

Method	HOG [11]	AL+HOG	HEP [12]	AL+HEP
AUC	0.840±0.060	0.864±0.071	0.856 ±0.078	**0.871 ±0.057**
$\bar{P}$(%)	73.5±8.5	76.9±8.9	76.9 ±8.8	**78.0 ±8.6**

The results shown in Table 1 indicate the following:

1. Comparing the classification accuracy of each individual method before and after axial alignment, we can see that both methods gain a certain improvement, which demonstrates that the proposed axial alignment has the ability to improve angle closure detection accuracy. Specifically, the HOG based method improves 2.9 % and HEP improves 1.8 % in terms of AUC, which might be explained as HOG being relatively more sensitive to rotation compared to HEP.
2. Comparing the two methods under the same axial alignment condition (with/without), HEP features outperform HOG features, which was also observed in [12]. This might be because HEP is extracted from down-sampled images with very low resolution, and thus has larger tolerance to rotational and translational misalignment.

4 Conclusion

In this work, we proposed a one-step method based on robust low-rank tensor recovery to solve the new yet fundamental axial alignment problem for AS-SS-OCT imaging. The preliminary experiments on angle closure analysis demonstrate that our proposed method not only can facilitate manual qualitative assessments, but also can significantly improve the accuracy of automatic quantitative assessments. This method thus exhibits much promise for other clinical applications besides anterior segment analysis.

References

1. Gora, M., Karnowski, K., Szkulmowski, M., Kaluzny, B.J., Huber, R., Kowalczyk, A., Wojtkowski, M.: Ultra high-speed swept source OCT imaging of the anterior segment of human eye at 200 kHz with adjustable imaging range. Opt. Express **17**(17), 14880–14894 (2009)
2. Lim, S.H.: Clinical applications of anterior segment optical coherence tomography. J. Ophthalmol. Article ID 605729, 12 (2015)
3. Maslin, J.S., Barkana, Y., Dorairaj, S.K.: Anterior segment imaging in glaucoma: an updated review. Indian J. Ophthalmol. **63**(8), 630–640 (2015)
4. Sakata, L.M., Lavanya, R., Friedman, D.S., Aung, H.T., Seah, S.K., Foster, P.J., Aung, T.: Assessment of the scleral spur in anterior segment optical coherence tomography images. Arch Ophthalmol. **126**(2), 181–185 (2008)
5. Mishima, K., Tomidokoro, A., Suramethakul, P., Mataki, N., Kurita, N., Mayama, C., Araie, M.: Iridotrabecular contact observed using anterior segment three-dimensional OCT in eyes with a shallow peripheral anterior chamber. Invest. Ophthalmol. Vis. Sci. **54**(7), 4628–4635 (2013)
6. Li, P., Johnstone, M., Wang, R.K.: Full anterior segment biometry with extended imaging range spectral domain optical coherence tomography at 1340 nm. J. Biomed. Opt. **19**(4), 046013 (2014)
7. The cornea/anterior segment OCT SS-1000 'CASIA'. http://www.tomey.com/Products/OCT/SS-1000CASIA.html

8. Xu, J., Ishikawa, H., Wollstein, G., Kagemann, L., Schuman, J.S.: Alignment of 3-D optical coherence tomography scans to correct eye movement using a particle filtering. IEEE Trans. Med. Image **31**(7), 1337–1345 (2012)
9. Montuoro, A., Wu, J., Waldstein, S., Gerendas, B., Langs, G., Simader, C., Schmidt-Erfurth, U.: Motion artefact correction in retinal optical coherence tomography using local symmetry. In: Golland, P., Hata, N., Barillot, C., Hornegger, J., Howe, R. (eds.) MICCAI 2014, Part II. LNCS, vol. 8674, pp. 130–137. Springer, Heidelberg (2014)
10. Navarro, R., González, L., Hernández, L.: Optics of the average normal cornea from general and canonical representations of its surface topography. J. Opt. Soc. Am. A. Opt. Image Sci. Vis. **23**(2), 219–232 (2006)
11. Xu, Y., Liu, J., Tan, N.M., Lee, B.H., Wong, D.W.K., Baskaran, M., Perera, S., Aung, T.: Anterior chamber angle classification using multiscale histograms of oriented gradients for glaucoma subtype identification. In: IEEE Engineering in Medicine and Biology Society, pp. 3167–3170 (2012)
12. Xu, Y., Liu, J., Cheng, J., Lee, B.H., Wong, D.W.K., Baskaran, M., Perera, S., Aung, T.: Automated anterior chamber angle localization and glaucoma type classification in OCT images. In: IEEE Engineering in Medicine and Biology Society, pp. 7380–7383 (2013)
13. Liu, J., Musialski, P., Wonka, P., Ye, J.: Tensor completion for estimating missing values in visual data. IEEE Trans. Pattern Anal. Mach. Intell. **35**(1), 208–220 (2013)
14. Kolda, T., Bader, B.: Tensor decompositions and applications. SIAM Rev. **51**(3), 455–500 (2009)
15. Xu, Y., Liu, J., Wong, D.W.K., Baskaran, M., Perera, S., Aung, T.: Similarity-weighted linear reconstruction of anterior chamber angles for glaucoma classification. In: IEEE International Symposium on Biomedical Imaging, pp. 693–697 (2016)
16. Peng, Y., Ganesh, A., Wright, J., Ma, Y.: RASL: robust alignment by sparse and low-rank decomposition for linearly correlated images. In: CVPR, pp. 2233–2246 (2013)
17. Lin, Z., Chen, M., Wu, L., Ma, Y.: The augmented lagrange multiplier method for exact recovery of corrupted low-rank matrices. UIUC Technical report UILU-ENG-09-2215 (2009)
18. Yang, J., Yuan, X.: Linearized augmented lagrangian and alternating direction methods for nuclear norm minimization. Math. Comput. **82**(281), 301–329 (2013)